

Naval Research Laboratory

Washington, DC 20375-5000



NRL Memorandum Report 6425

AD-A206 348

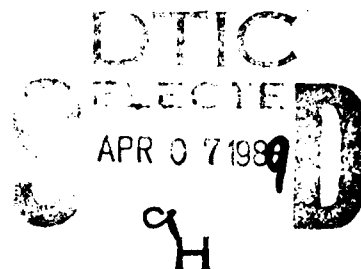
Simulation Studies of Particle Acceleration Powered by Modulated Intense Relativistic Electron Beams

J. KRALL*, V. SERLIN, M. FRIEDMAN AND Y. Y. LAU

**Science Applications Intl. Corp.,
McLean, VA*

*Plasma Theory Branch
Plasma Physics Division*

March 14, 1989



Approved for public release; distribution unlimited.

39 4 07 035

SECURITY CLASSIFICATION OF THIS PAGE

ADA206348

REPORT DOCUMENTATION PAGE				Form Approved OMB No 0704-0188	
1a REPORT SECURITY CLASSIFICATION UNCLASSIFIED			1b RESTRICTIVE MARKINGS		
2a SECURITY CLASSIFICATION AUTHORITY			3 DISTRIBUTION/AVAILABILITY OF REPORT Approved for public release; distribution unlimited.		
2b DECLASSIFICATION/DOWNGRADING SCHEDULE			5 MONITORING ORGANIZATION REPORT NUMBER(S)		
4 PERFORMING ORGANIZATION REPORT NUMBER(S) NRL Memorandum Report 6425			7a NAME OF MONITORING ORGANIZATION		
6a NAME OF PERFORMING ORGANIZATION Naval Research Laboratory		6b OFFICE SYMBOL (If applicable) Code 4790		7b ADDRESS (City, State, and ZIP Code)	
6c ADDRESS (City, State, and ZIP Code) Washington, DC 20375-5000			9 PROCUREMENT INSTRUMENT IDENTIFICATION NUMBER		
8a NAME OF FUNDING SPONSORING ORGANIZATION U.S. Department of Energy		8b OFFICE SYMBOL (If applicable)		10 SOURCE OF FUNDING NUMBERS	
8c ADDRESS (City, State, and ZIP Code) Washington, DC 20545			PROGRAM ELEMENT NO DOE		PROJECT NO AI05-86 TASK NO ER23585 WORK UNIT ACCESSION NO
11 TITLE (Include Security Classification) Simulation Studies of Particle Acceleration Powered by Modulated Intense Relativistic Electron Beams					
12 PERSONAL AUTHOR(S) Krall,* J., Serlin, V., Friedman, M. and Lau, Y.Y.					
13a TYPE OF REPORT Interim		13b TIME COVERED FROM _____ TO _____		14 DATE OF REPORT (Year, Month, Day) 1989 March 14	
15 PAGE COUNT 39					
16 SUPPLEMENTARY NOTATION *Science Applications Intl. Corp., McLean, VA					
17 COSATI CODES			18 SUBJECT TERMS (Continue on reverse if necessary and identify by block number)		
FIELD	GROUP	SUB-GROUP	Particle accelerators Intense relativistic elec.		
			Compact accelerators beams		
			Particle simulations		
19 ABSTRACT (Continue on reverse if necessary and identify by block number) A time dependent, fully electromagnetic particle code is used to simulate transfer of energy from an annular modulated intense relativistic electron beam to a low current electron beam via a disk-loaded structure. It is shown that an intense beam may be used to drive such an accelerator at high transformer ratio ($R = 10$) to obtain accelerating gradients in the ~ 100 Mv/m range, with power in excess of 1 GW transferred from the primary to the secondary beam.					
20 DISTRIBUTION AVAILABILITY OF ABSTRACT <input checked="" type="checkbox"/> UNCLASSIFIED UNLIMITED <input type="checkbox"/> SAME AS RPT <input type="checkbox"/> DTIC USERS			21 ABSTRACT SECURITY CLASSIFICATION UNCLASSIFIED		
22a NAME OF RESPONSIBLE INDIVIDUAL Y. Y. Lau			22b TELEPHONE (Include Area Code) (202) 767-2765		22c OFFICE SYMBOL Code 4790

DD Form 1473, JUN 86

Previous editions are obsolete

SECURITY CLASSIFICATION OF THIS PAGE

S/N 0102-LF-014-6603

CONTENTS

I.	INTRODUCTION	1
II.	FIELDS IN THE RF STRUCTURE	3
III.	NUMERICAL SIMULATIONS	5
IV.	NUMERICAL EFFECTS	10
V.	CONCLUSIONS	11
	ACKNOWLEDGEMENTS	12
	REFERENCES	13
	DISTRIBUTION LIST	29



Accession For		
NTIS (EASI)	<input checked="" type="checkbox"/>	
DTIC TAB	<input type="checkbox"/>	
Unannounced	<input type="checkbox"/>	
Justification		
By		
Initials / Date		
Availability Codes		
Available / or		
Dist	Original	
A-1		

SIMULATION STUDIES OF PARTICLE ACCELERATION POWERED BY MODULATED INTENSE RELATIVISTIC ELECTRON BEAMS

I. Introduction

Future progress in accelerators and their applications may depend critically on the development of physical mechanisms capable of generating high voltage gradients. It has been shown that a high electric field can be established in rf structures by modulated intense relativistic electron beams (MIREBs) of power greater than 10^9 W and that such a beam may be used as an rf source to power an accelerator, obtaining voltage gradients as high as 100 MeV/m or greater.^{1,2} Such accelerators, in which a low power, high current beam interacts via a metallic structure with a low current beam to obtain very high energies have been suggested by a number of authors, including Voss and Weiland,³ in addition to the accelerator outlined in Ref. 2. Wakefield acceleration has recently been observed in experiments carried out by Figueroa et al.⁴

Theoretical discussions of accelerators powered by MIREBs^{2,5} have suggested unusual properties that may be present in the following devices: Firstly, the demonstrated conversion of the high dc power of an intense relativistic electron beam (IREB) to high rf power in the MIREB by the use of tuned radial cavities implies that the MIREB may be coupled to an rf structure so as to drain significant power (> 1 GW) from the beam at high efficiency and, secondly, geometrical effects may allow for sizeable variations in efficiency, field gradient, and coupling between the high power MIREB and the rf structure with small changes in the experimental parameters.

In the present paper we study these issues via an axisymmetric particle simulation using the CONDOR⁶ code, which has been previously and successfully applied to the physics of such intense beams.⁷ The accelerator configuration to be studied is similar to that outlined in Ref. 2 and is pictured in Fig. 1.

(1) An annular IREB generator injects a beam of radius $r_b \approx 6.3$ cm, current $I_o = 16$ kA, energy $E_{inj} = 500$ keV and duration $T = 150$ ns into a drift tube of radius $r_w \approx 6.8$ cm. The IREB is guided by an axial field, $B_o = 10$ kG.

(2) The IREB is fully modulated at $f \approx 1.3$ GHz by a pair of tuned radial cavities, the first of which is externally driven by a low level rf source (magnetron). The modulation region is immersed in the axial magnetic field.

(3) The MIREB is guided into a cylindrical cavity of radius 9.6 cm. The cavity is loaded with thin disks of radius 9.0 cm and separation 1.88 cm. The MIREB, which has a frequency of modulation corresponding to the desired mode of the rf structure, is terminated at the first disk. A resonant interaction occurs at the gap defined by the end of the drift tube and the first disk of the rf structure, transferring energy from the beam to the rf structure.

(4) An emitter, located on-axis on the surface of the first disk, emits electrons when the fields within the structure reach a sufficiently high value. This secondary beam is then accelerated by the rf fields, guided by the axial magnetic field.

The modulation stage of this device has been studied in some detail for a 1.9 cm radius annular beam in a 2.4 cm radius drift tube^{5,7,8} and has been successfully repeated at $I_o = 16$ kA and $r_b = 6.3$ cm in a drift tube of radius 6.8 cm.⁹

In the present paper, we will investigate the coupling between the modulated beam and the rf structure and the subsequent acceleration of the secondary beam and shall proceed as follows. In Sec. II, we give theoretical background on the expected field gradients in the rf structure, define a transformer ratio for this acceleration scheme, and present

numerical results from the Superfish¹⁰ code on the modes of the rf structure. In Sec. III, which contains the main results of this paper, we will simulate particle acceleration and will see that power in excess of 1 GW may be transferred between the primary and secondary beams. Here we will consider the effect of geometrical variations on the beam-rf structure coupling and on the transformer ratio. Section IV will contain a detailed discussion of the numerical issues that effect the ability of these simulations to correctly predict experimental results. Section V concludes.

II. Fields in the RF Structure

The process of energy transfer between the primary and secondary beams in this accelerator resembles that of the wakefield schemes described in Refs. 3 and 4 in the use of fields excited by the primary beam in a disk loaded structure. In these schemes, the two beams travel colinearly such that the transformer ratio is defined as $R = E_2/E_1$ where E_1 is the magnitude of the decelerating field experienced by the primary beam and E_2 is the accelerating gradient experienced by secondary beam. In the present case, however, the interaction of the primary beam with the rf structure takes place only as the beam traverses the gap near the first disk of the rf structure, where the beam is terminated, while the secondary beam is accelerated along the entire length of the rf structure. The transformer ratio is then defined as

$$R = \frac{\langle E_{axis} \rangle L}{E_{gap} d}, \quad (1)$$

where d is the gap length, L is length of the rf structure, E_{gap} is the decelerating field in the gap (assumed spatially constant) and $\langle E_{\text{axis}} \rangle$ is the average field experienced by the accelerated secondary beam particles.

This geometry has been modelled as an interaction between a sinusoidally varying current source and a transmission line consisting of a series of R-L-C circuit elements.² This model exhibited many features that have been found in the numerical simulations, but such a model has a limited predictive capability.

Some insight into this problem may be obtained by assuming that the disk structure will behave like a resonant cavity. The normal modes of this cavity may be solved for by neglecting the interaction region at the gap.² For the purposes of this discussion, however, we may consider the only fundamental mode of a disk-loaded cavity of length $L = n\lambda/2$ where λ is the wavelength of the rf and n is a positive integer. In this case, the z -component of the electric field of the fundamental mode varies sinusoidally along the axis and radially as

$$E_z(r)/E_z(r=0) = J_0(kr)/J_0(r=0) , \quad (2)$$

where J_0 is a Bessel function and $k = 2\pi/\lambda$. In the analysis of Ref. 2, it was conjectured via a heuristic argument that the ratio of the field experienced at the gap by the primary beam, $r = r_b$, to the peak field on-axis, $r = 0$, would follow this radial variation. This suggests that the radial position of the primary beam in relation to the mode structure within the rf cavity is of some importance for the strength of the interaction, the efficiency, and the obtainable transformer ratio.

The normal modes for a given axisymmetric cavity may be calculated numerically by using the Superfish¹⁰ code. The Superfish result for one such cavity is shown in Fig. 2. Here, a disk loaded cavity of length $L \approx \lambda$

is used and the gap region is included. Except for the metallic boundary condition imposed at the right-hand wall, this geometry closely resembles that of Fig. 1, where the right-hand boundary is an open drift tube for which the 1.33 GHz cavity mode is below cutoff. This result and a series of similar results, where the location of the right-hand wall was varied, show that the expected cavity mode is obtained.

III. Numerical Simulations

The simulation geometry (Fig. 3) consists of a short drift tube region with radius $r_w = 6.8$ cm, a gap of length $d = 1.57$ cm and a disk-loaded structure of length $L = 22.2$ cm $\approx \lambda$, where $\lambda = c/f$, and $f = 1.27$ GHz is the frequency of the accelerating mode of the cavity, and was determined numerically.

The primary beam is injected from the left-hand wall with radius $r_b = 6.4$ cm, energy $E_{inj} = 2.0$ MeV and current $I_{inj}(kA) = g(t) [16 + 8\sin(2\pi ft)]$, where $g(t)$ is an envelope function that increases linearly from zero to unity during the time $0 < t < 15$ ns and remains constant thereafter. At a selected time, $t > 15$ ns, the secondary beam with $I_2 = 10$ Amperes and $E_2 = 0.1$ MeV is injected continuously from the center of the first disk and is accelerated along the axis by the rf fields. Each simulation continues until $t = 30$ ns.

Note that in order for the cavity-mode approximation of Sec. II to be of use the parameters L , v_g and T must be such that $L/v_g \ll T$, where v_g is the group velocity of E-M radiation within the disk-loaded structure and T is the duration of the primary beam pulse. If this relation is not satisfied, the disk structure will behave, not like a cavity, but like a travelling wave tube. In the numerical geometry of Fig. 3, we have arranged the separation between the outer disk edges and the cavity wall so

that $v_g/c \approx 1$. In this case the condition, $L/v_g \ll T$, is easily satisfied within the 30 ns duration of the simulations.

Several differences between this configuration and that of a practical experiment must be noted.

(1) In a practical experiment the disk structure would be longer so as to obtain higher energies in the secondary beam. Another difficulty is that the high group velocity of the E-M waves in the simulation structure and its short length and small volume would allow rf fields to build up so quickly that they might reflect the primary beam in an actual device.

(2) An actual device would have support rods to hold the disks in place. These would also provide a path for the dc current of the primary beam. Because such supports cannot be modelled axisymmetrically and because we require a dc current path, we inserted a center conductor to serve this purpose. It will be seen in Sec. IV, below, that the presence of this center conductor does not significantly effect the results.

(3) In the simulation geometry, the left-hand boundary is a metallic wall. In an actual device and in Fig. 1, this boundary is an open drift tube, for which the 1.27 GHz frequency of the rf field is below cutoff. The metal boundary of the simulations will have the similar effect of reflecting incident radiation at this frequency, but is clearly not the same.

(4) The simulation structures are defined on a grid such that the effective skin depth of the material is one grid cell ($\Delta r = 0.2$ cm, $\Delta z = 0.3133$ cm), making the cavity extremely lossy, with Q of order 10. A typical value for a metallic structure is of order 1000.

Figures 4 and 5 show the z-component of the electric field plotted vs. time in the gap and on-axis, respectively, for a simulation with parameters

described above. The plot on-axis is taken at the spatial location of the peak electric field. We see that the fields increase continuously, reaching values of 56.3 MV/m at the gap and 94.2 MV/m on-axis before the simulation is halted. The plot of the gap electric field shows evidence of a weak, lower frequency mode which may have been excited by the increase in dc current from $t = 0$ to $t = 15$ ns. The rf cavity mode, as expected, is a standing wave, varying sinusoidally in z and as a Bessel function, $J_0(kr)$, radially. This is seen in Figs. 6 and 7 which show E_z vs. z and E_z vs. r , respectively, at fixed time.

For the simulation shown, the secondary beam was injected continuously for $t > 17$ ns with $I_2 = 10$ A and $E_2 = 0.1$ MeV and was bunched and accelerated by the rf fields. This acceleration may be observed in Fig. 8, which plots particle positions in phase space, $\gamma\beta c$ vs. z , where β is the axial particle velocity normalized to c and $\gamma = (1 - \beta^2)^{-1/2}$. The particle positions, plotted at fixed time at intervals of 0.2 ns, show a maximum energy increase of 8.60 MeV over 22.2 cm to give an accelerating gradient of 39.2 MV/m. With this result and the observed 56.3 MV/m at the gap, we see that for this case a transformer ratio $R = 9.85$ has been achieved.

Several interesting aspects of this simulation should be noted.

(1) The build-up of rf in the cavity is of a transient nature. Were the simulation not halted at $t = 30$ ns, the field amplitudes would increase beyond the observed 94.2 MV/m until limited by reflection of the primary beam. In an actual device, other limitations may include breakdown in the rf structure, losses due to the Q of the cavity, termination of the primary beam, or acceleration of a sufficiently high quantity of secondary beam current.

(2) The conjectured relationship between the gap field, E_{gap} , and the peak axial field, E_{axis} , which was discussed in connection with Eq. (2) above, does not hold. Here, we have $E_{\text{axis}}/E_{\text{gap}} = 1.67$ and $J_0(0)/J_0(kr_b) = 2.51$. While the conjectured relation does not hold in a precise way, it may still be useful as a qualitative guide. We still expect that an increase in $J_0(0)/J_0(kr_b)$, obtainable by increasing r_b , will result in an increased $E_{\text{axis}}/E_{\text{gap}}$. This will be investigated below.

(3) The electric field of 56.3 MV/m that is observed across the 1.57 cm gap indicates that the primary beam loses 0.883 MV as it traverses the gap. This energy loss is verified in the phase-space plots of Fig. 8, where the primary beam particles, which have $0 < z < 10$ cm, are deflected in momentum space by the gap voltage. This indicates a power drain of 7.07 GW at 1.27 GHz and is sufficient power to accelerate secondary beam current in the 500 A range over this short distance. With a longer accelerating structure, lower currents may be accelerated to higher energies.

To test our conjecture that higher current may be accelerated to obtain high power in the secondary beam, we repeated the simulation of Figs. 4-8 with the secondary beam current increased to 200 A. We found $E_{\text{gap}} = 51.6$ MV/m and $E_{\text{axis}} = 91.3$ MV/m. Secondary beam particles, injected at 0.1 MeV, were accelerated to 8.02 MeV to give $\langle E_{\text{axis}} \rangle = 35.7$ MV/m so that $R = 9.78$. A comparison of these results with those of Figs. 4-8 indicates that the 200 A secondary beam does not significantly load the cavity. We also see that 1.58 GW of rf power has been transferred from the primary to the secondary beam.

While the supposed relationship between E_{gap} and E_{axis} discussed in connection with Eq. (2) has already been proven imprecise, the possibility of obtaining very high transformer ratios as the primary beam radius

approaches $r_b = j_{0,1}/k$, where $J_0(j_{0,1}) = 0$, remains intriguing. We investigated this by repeating the simulation of Figs. 4-8 with $r_b = 8.0$ cm. This necessitated an increase in the drift tube radius to $r_w = 8.4$ cm, a change in geometry which shifted the resonance slightly to 1.34 GHz. At this frequency, $j_{0,1}/k = 8.57$ cm. The results of the simulation are shown in Figs. 9-12. We found field gradients of $E_{\text{gap}} = 13.5$ MV/m and $E_{\text{axis}} = 34.4$ MV/m. Particle plots (not shown) indicated that the secondary beam particles, injected at 0.1 MeV, were accelerated to 3.27 MeV to give $\langle E_{\text{axis}} \rangle = 14.3$ MV/m so that R has been increased to 15.0. Figures 9-12 contain the following results:

(1) With $r_b = 8.0$, we have $E_{\text{axis}}/E_{\text{gap}} = 2.55$, an increase from the value of 1.67 that was obtained at $r_b = 6.4$ cm, but not nearly as large as $J_0(0)/J_0(kr_b) = 11.9$. Note that the transformer ratio was similarly increased, from 9.85 to 15.0. As stated above, we have only a qualitative ability to predict results as r_b is changed.

(2) Figures 9 and 10 show that the build-up of rf fields in the cavity is of a transient nature, as before, but much lower amplitudes are reached at $t = 30$ ns than in the $r_b = 6.4$ cm case. This indicates that as the $E_{\text{axis}}/E_{\text{gap}}$ ratio is increased, the interaction between the primary beam and the rf structure is weakened. This occurs because, at a higher transformer ratio, the same accelerating field in the rf structure gives a lower decelerating field at the gap and less energy is drained from the primary beam per cycle. The low frequency excitation of the cavity, apparent in Figs. 4 and 9, is unchanged, making it more prominent in the latter case where the rf fields are weaker.

(3) The peak electric field on-axis, plotted in Fig. 10, appears to be saturating as the simulation is terminated. It is not clear whether this is a result of the low Q of the numerical structure or if we are driving

the cavity slightly off resonance. We can also see, from Figs. 11 and 12, that the mode structure is unchanged from the previous cases.

Finally, we must note that at $r_w = 8.4$ cm, $f = 1.34$ GHz is very close to the cutoff frequency, $f_c = j_{0,1}c/2\pi r_w = 1.37$ GHz. In a practical device, it may not be possible to increase r_b and r_w to such large values at this frequency.

IV. Numerical Effects

To understand the applicability of the simulation results to an actual device, it is necessary to examine the differences between such a device and the numerical model. Many of these have already been addressed. One which was not is the addition of a center conductor to the drift tube region of the simulation geometry, which provides a path for the dc component of the primary beam current. The significance of this addition may be examined by considering equivalent circuit elements for the rf structure, a capacitive load, and the center conductor, an inductive load. These elements are connected in parallel and are driven by an oscillatory current source. The inductance of a coaxial line varies as $L \propto \log(r_w/r_c)$, where r_c is the radius of the center conductor. The equivalent circuit model suggests that an increase in r_c will lower the inductive load relative to the capacitive load, lowering the voltage across the capacitance. This was verified by increasing the radius of the center conductor to $r_c = 5.0$ cm in the $r_b = 6.4$ cm case. This had the effect of lowering the field amplitudes in the gap and on-axis by a factor of 1.7, but left the transformer ratio unchanged. Conversely, the circuit model suggests that for sufficiently small values of r_c , the inductance will be so high that it will behave as an open circuit. In this ideal case, the entire load lies across the capacitance.

To discover whether or not the radius of the center conductor is sufficiently small, we repeated the $r_b = 6.4$ cm simulation with the dc component of the primary beam current removed, so that $I_{inj}(kA) = g(t)8\sin(2\pi ft)$, where $g(t)$ is an envelope function as before. This was accomplished by superimposing an appropriately modulated electron beam with a dc positron beam, and allowed us to compare results with and without the presence of the center conductor. With the center conductor, we found $E_{gap} = 56.1$ MV/m, $E_{axis} = 92.6$ MV/m and $\langle E_{axis} \rangle = 38.8$ MV/m, comparable to the results of Figs. 4-8. Without the center conductor, we found $E_{gap} = 60.0$ MV/m, $E_{axis} = 103.6$ MV/m and $\langle E_{axis} \rangle = 41.5$ MV/m. This indicates that the presence of the center conductor reduces the fields by 5-10 %.

V. Conclusions

We have demonstrated that high fields and transformer ratios can be supported by a MIREB-driven accelerator, with several interesting properties. The most crucial of these is that the MIREB is so strongly coupled to the disk-loaded rf structure that power in excess of 1 GW may be transferred from the primary to the secondary beam, despite the low Q of the numerical structure.

We have found that the build-up of the rf fields in the structure is transient by nature and, in the simulations, peak accelerating gradients were limited only by the brevity of the simulations. In an actual device, these fields will continue to increase in amplitude until limited by breakdown in the rf structure, reflection of the primary beam at the gap or by termination of the primary beam pulse.

We have also considered variations of the geometry to successfully obtain an increased transformer ratio, but at the cost of weakening the coupling between the primary beam and the rf structure. We have also found

that the conjectured relationship between the decelerating field experienced by the primary beam at the gap and the peak accelerating gradient on-axis, which is discussed in connection with Eq. (2), provides only a qualitative guide to these geometric variations. As the original conjecture, contained in Ref. 2, is heuristic in nature and pertains to an idealized physical model, this is not a surprising result.

Finally, the differences between these simulations and a practical experimental configuration have been discussed in some detail, suggesting that similar power levels, fields and transformer ratios may be obtainable experimentally.

Acknowledgements

This work was supported by the Department of Energy under Contract No. DE-AI05-86-ER13585.

References

1. M. Friedman and V. Serlin, Phys. Rev. Lett. 55, 2860 (1985).
2. M. Friedman and V. Serlin, Appl. Phys. Lett. 49, 596 (1986).
3. G. Voss and T. Weiland, Desy Report M82-10 and Desy Report M82079, 1982.
4. H. Figueroa, W. Gai, R. Konecny, J. Norem, A. Ruggiero, P. Schoessow and J. Simpson, Phys. Rev. Lett. 60, 2144 (1988).
5. M. Friedman, J. Krall, Y.Y. Lau and V. Serlin, J. Appl. Phys. 64, 3353 (1988).
6. CONDOR is an extension of the MASK particle code, discussed in A. Palevsky and A. Drobot, in Proceedings of the 9th Conference on Numerical Simulation of Plasmas, July 1980 (Northwestern University, Evanston, IL) (unpublished).
7. J. Krall and Y.Y. Lau, Appl. Phys. Lett. 52, 431 (1988).
8. Y.Y. Lau, J. Krall, M. Friedman and V. Serlin, IEEE Trans. Plas. Sci. 16-2, 249 (1988).
9. M. Friedman, V. Serlin, Y.Y. Lau and J. Krall, to be published.
10. K. H. Halbach and R. F. Holsinger, LBL report LBL-5040, 1976.

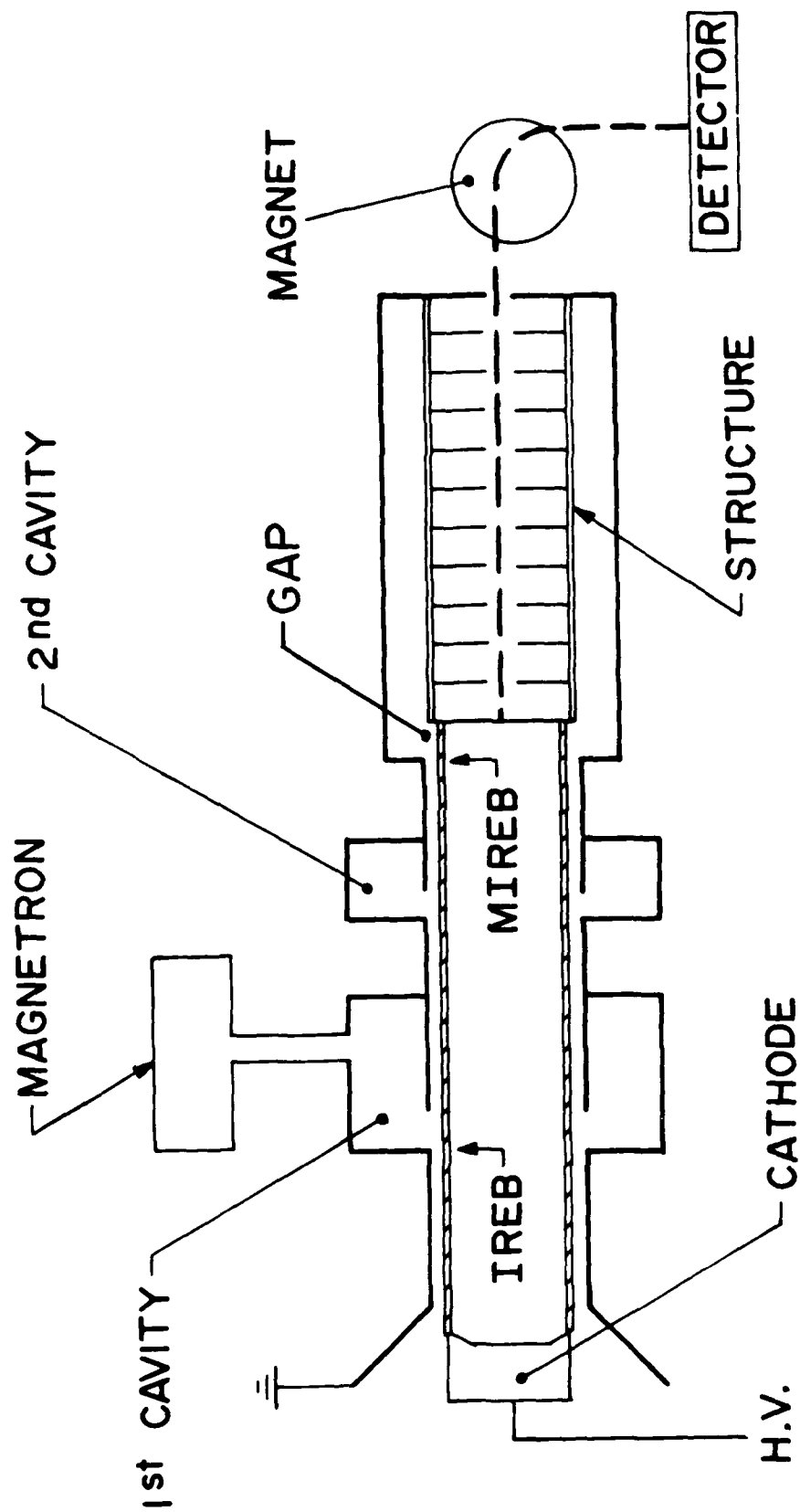


Fig. 1. MIREB-driven accelerator schematic.

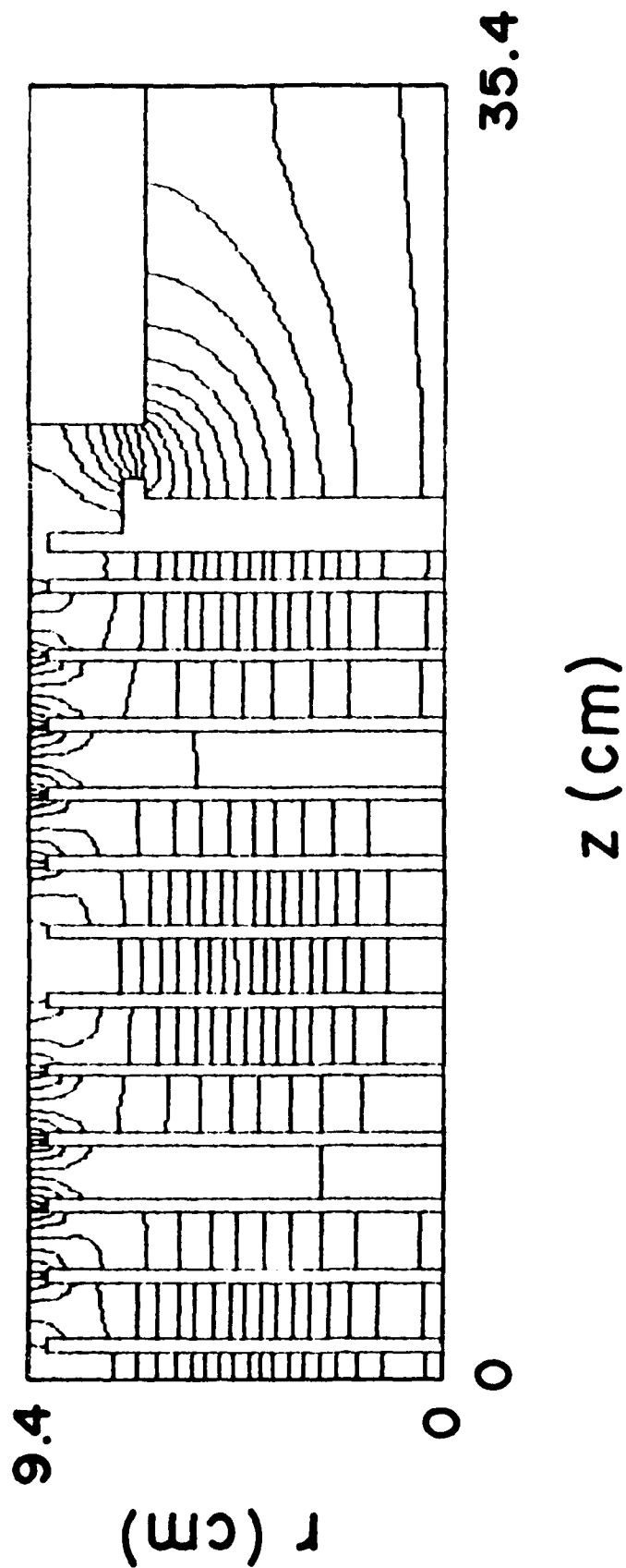


Fig. 2. Superfish result showing the electric field configuration of an rf structure cavity mode with frequency 1.33 GHz.

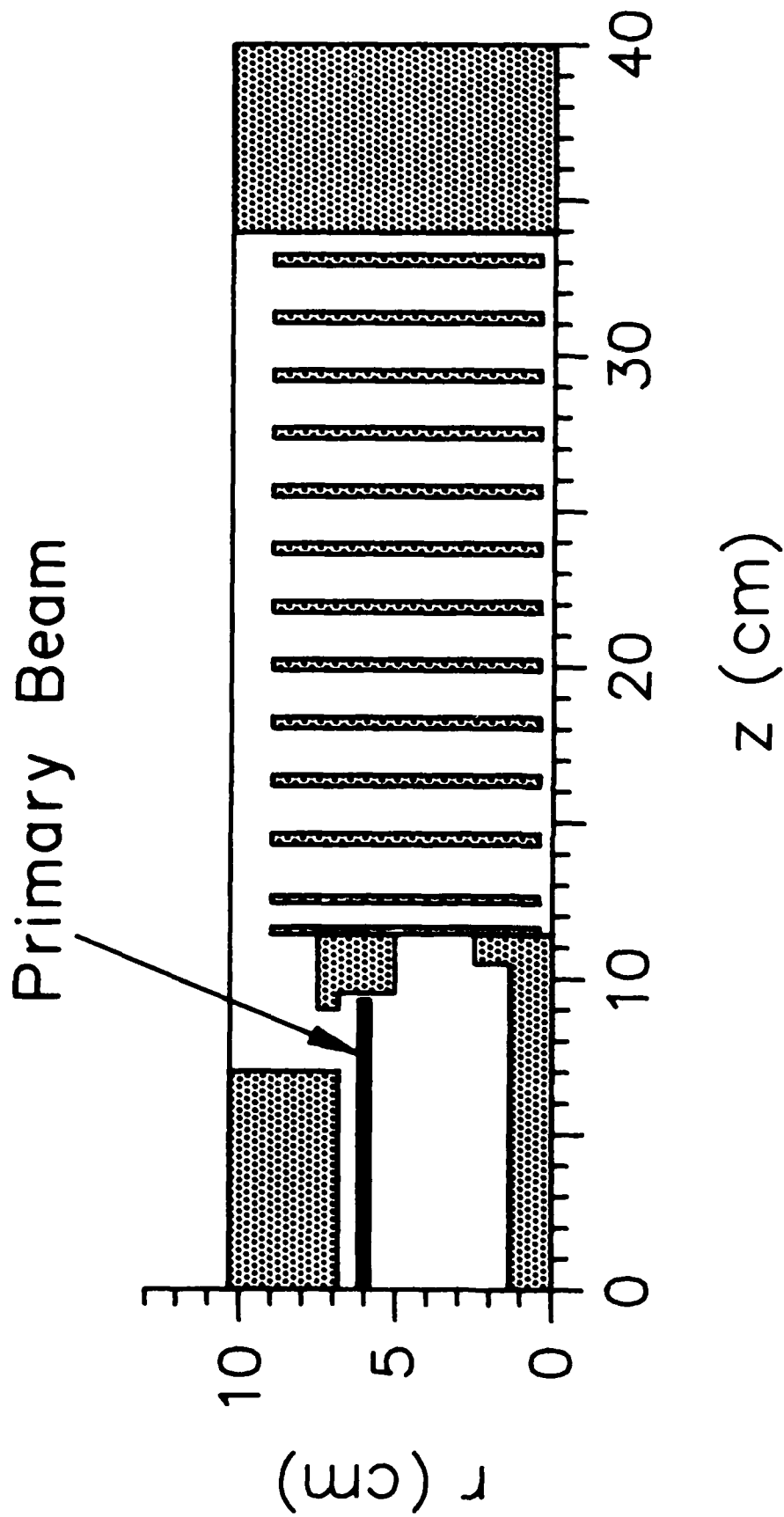


Fig. 3. Simulation geometry showing the primary beam and the disk-loaded rf structure. The primary beam enters the drift tube region from the left, passes near the gap at $z \approx 8$ cm and is terminated at $z \approx 9$ cm. The secondary beam is injected at $z \approx 12$ cm and is accelerated along the axis.

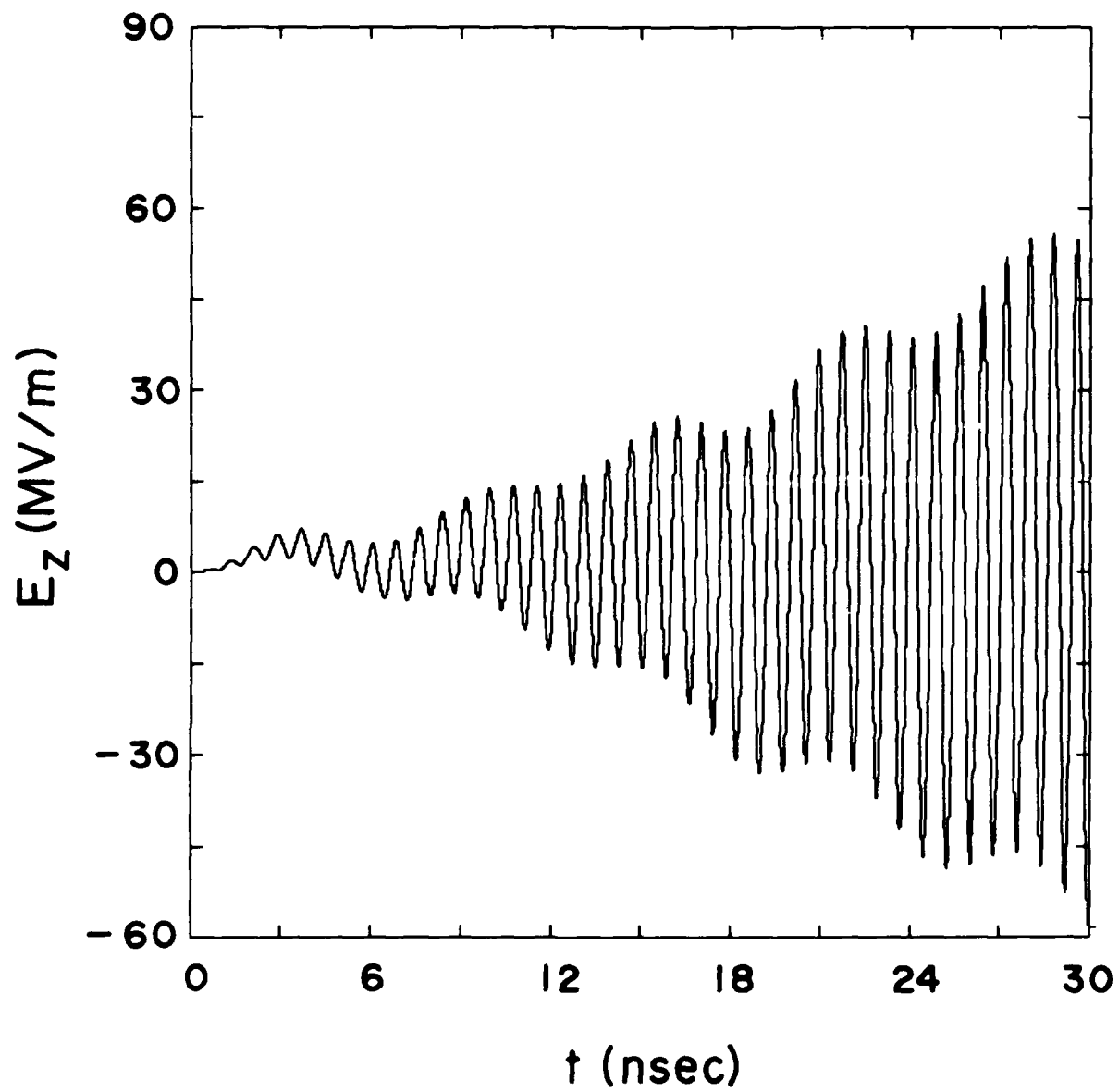


Fig. 4. E_z plotted versus time at the gap for the $r_b = 6.4$ cm case.

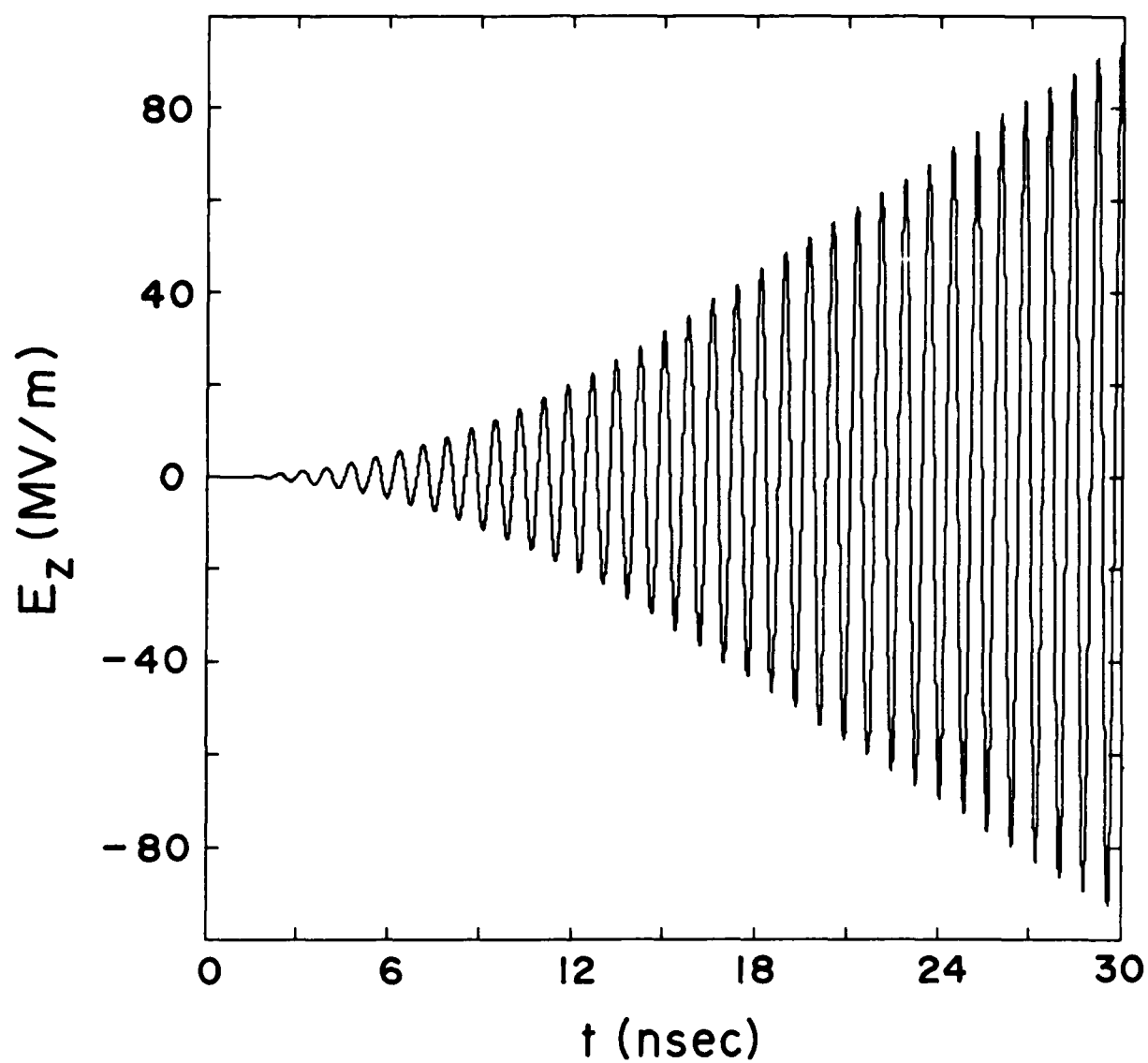


Fig. 5. E_z versus time on-axis at $z = 20.6$ cm, near the point of peak axial field.

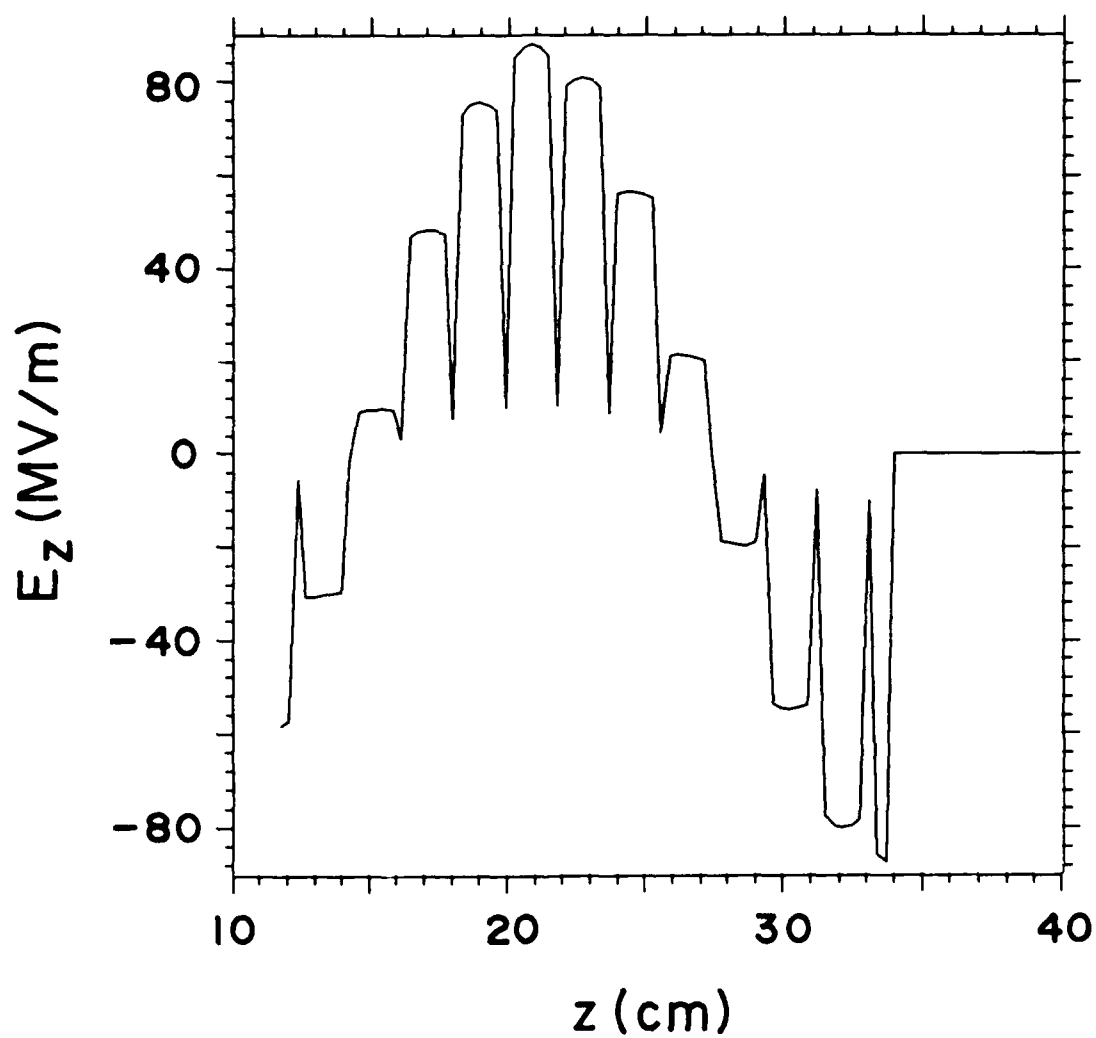


Fig. 6. E_z versus z plotted on-axis at $t = 28.4$ ns.

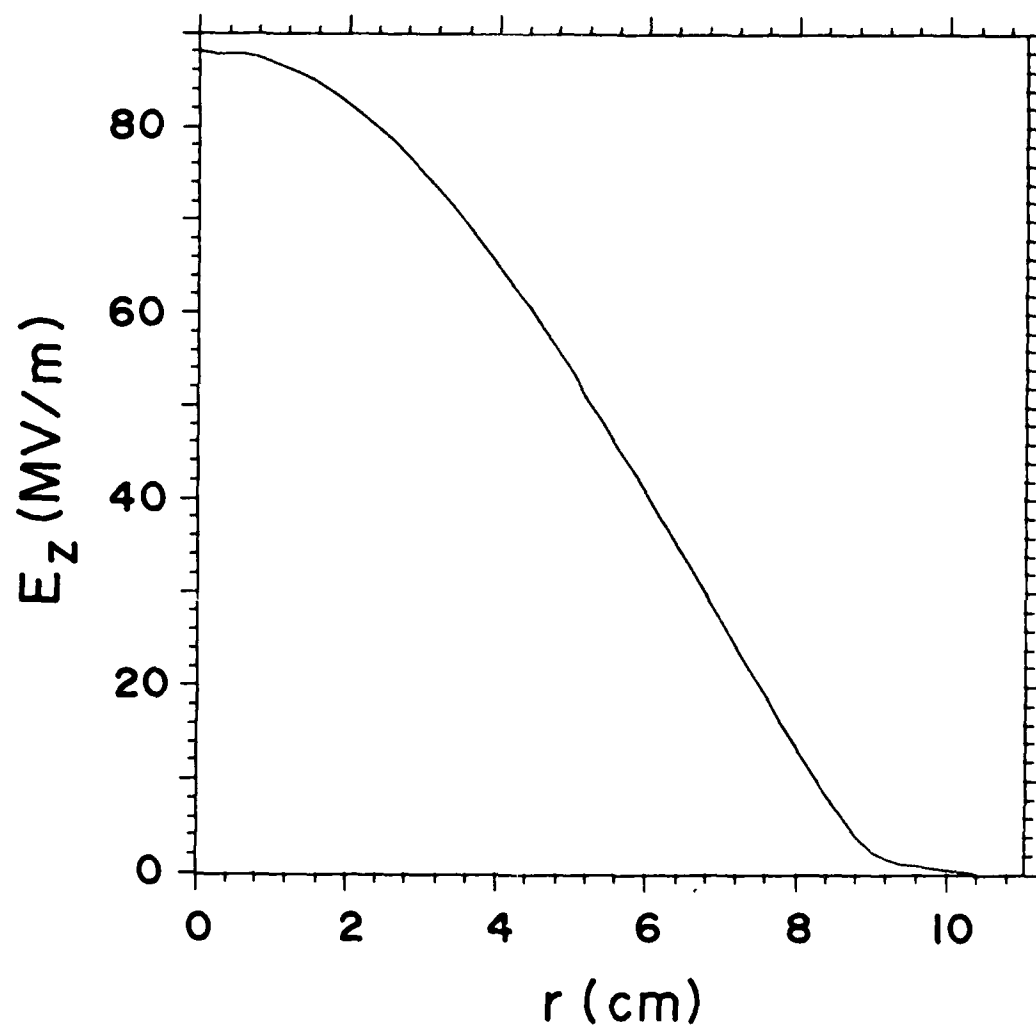


Fig. 7. E_z versus r plotted near the point of peak axial field, $z = 20.6$ cm, at $t = 28.4$ ns.

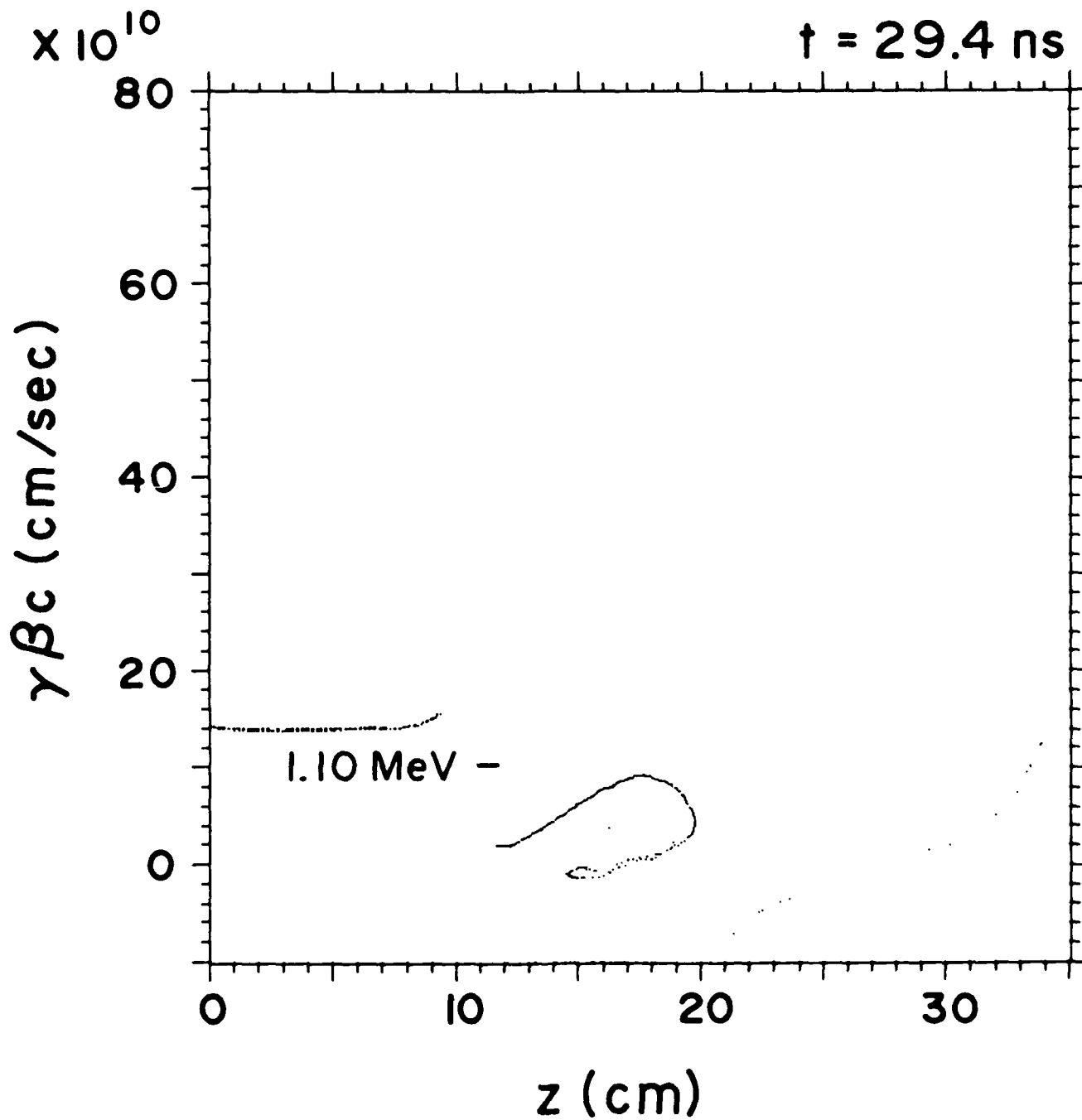


Fig. 8 — Particle positions in phase-space, $\gamma\beta_z c$ versus z , at intervals of 0.2 ns. The primary beam is on the left, $0 < z < 10$ cm. The peak energy of the accelerating secondary beam particles is noted on each plot.

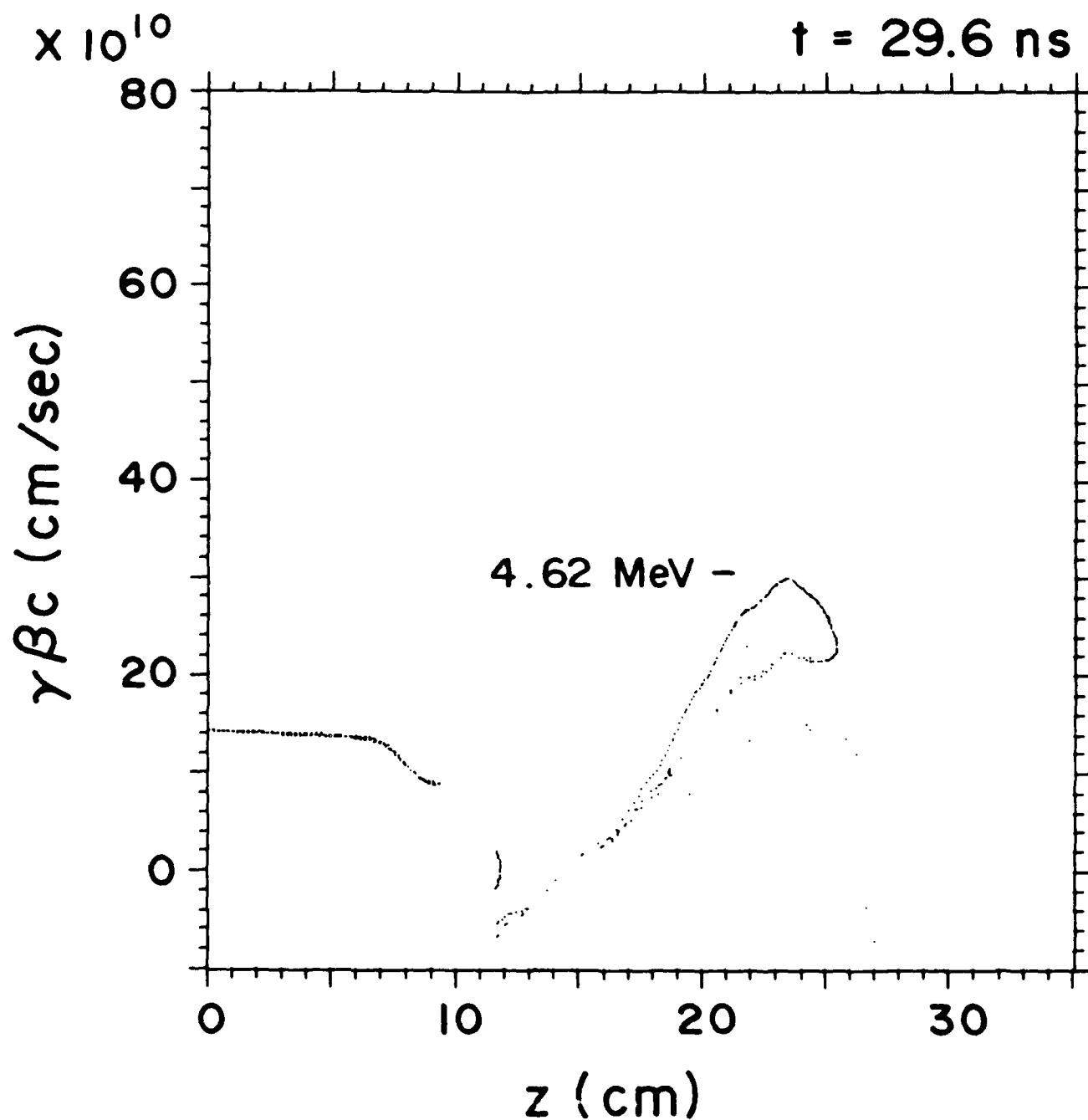


Fig. 8 (Continued) — Particle positions in phase-space, $\gamma\beta_z c$ versus z , at intervals of 0.2 ns. The primary beam is on the left, $0 < z < 10$ cm. The peak energy of the accelerating secondary beam particles is noted on each plot.

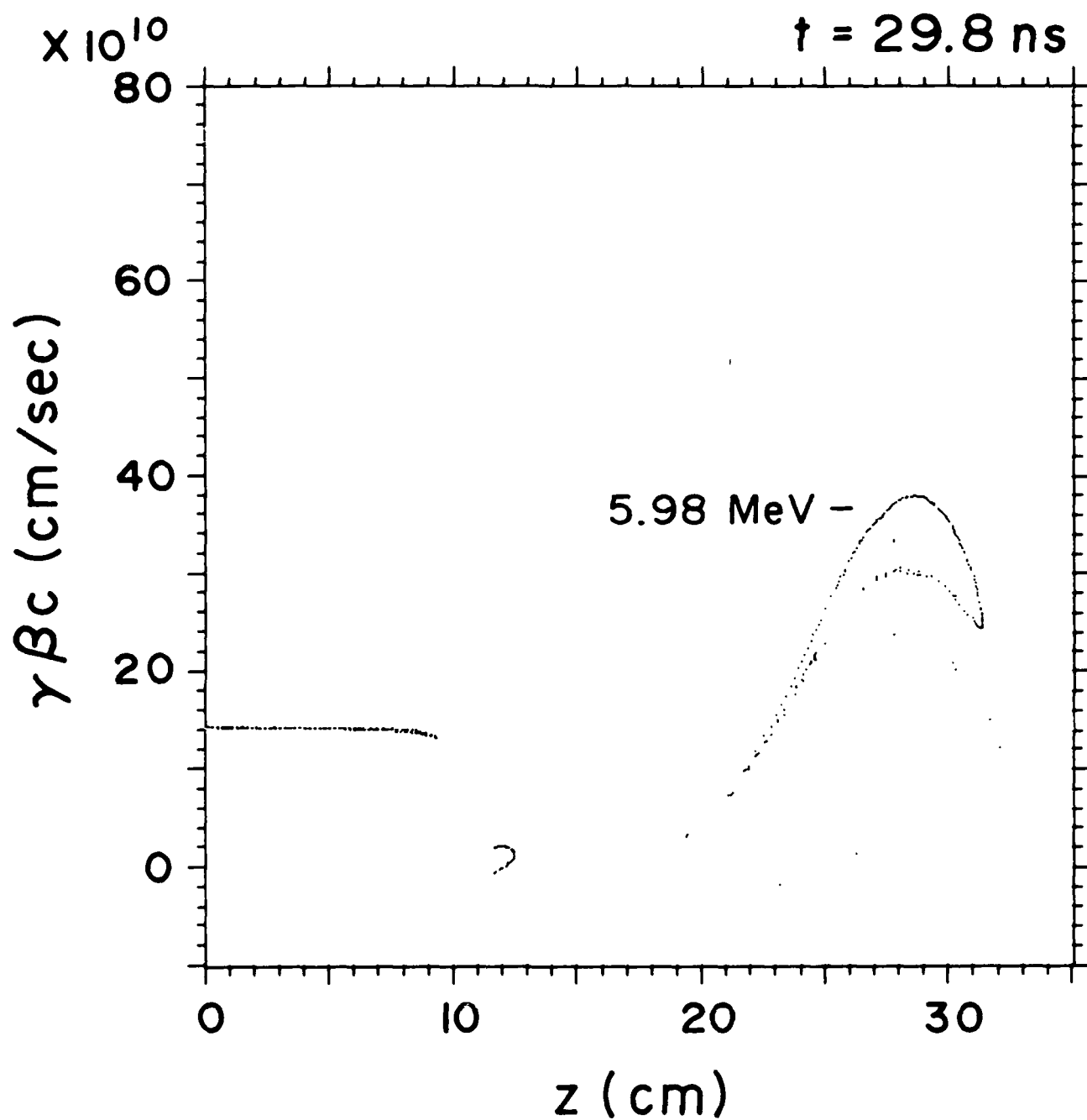


Fig. 8 (Continued) — Particle positions in phase-space, $\gamma\beta c$ versus z , at intervals of 0.2 ns. The primary beam is on the left, $0 < z < 10$ cm. The peak energy of the accelerating secondary beam particles is noted on each plot.

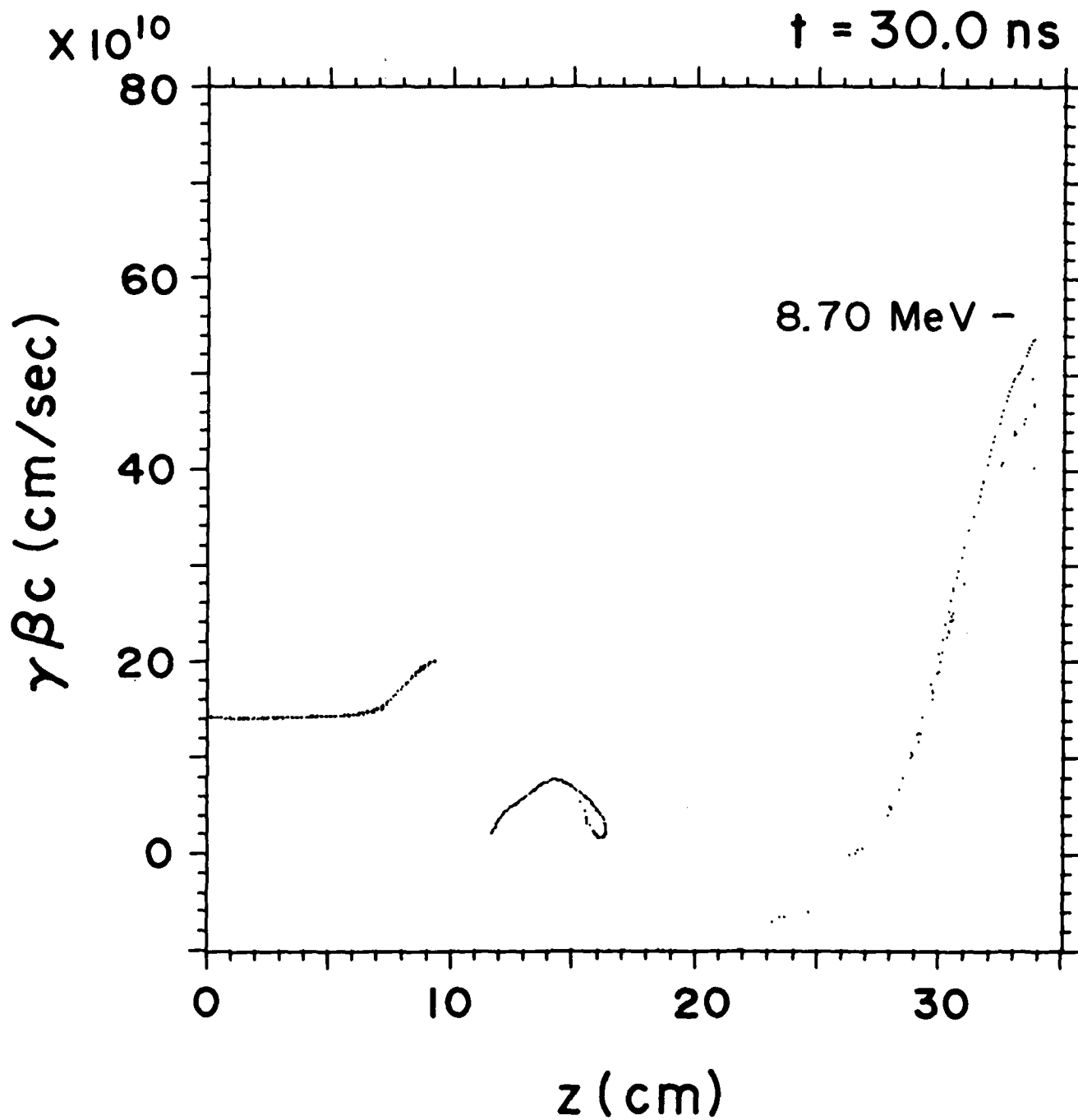


Fig. 8 (Continued) — Particle positions in phase-space, $\gamma\beta_z c$ versus z , at intervals of 0.2 ns. The primary beam is on the left, $0 < z < 10 \text{ cm}$. The peak energy of the accelerating secondary beam particles is noted on each plot.

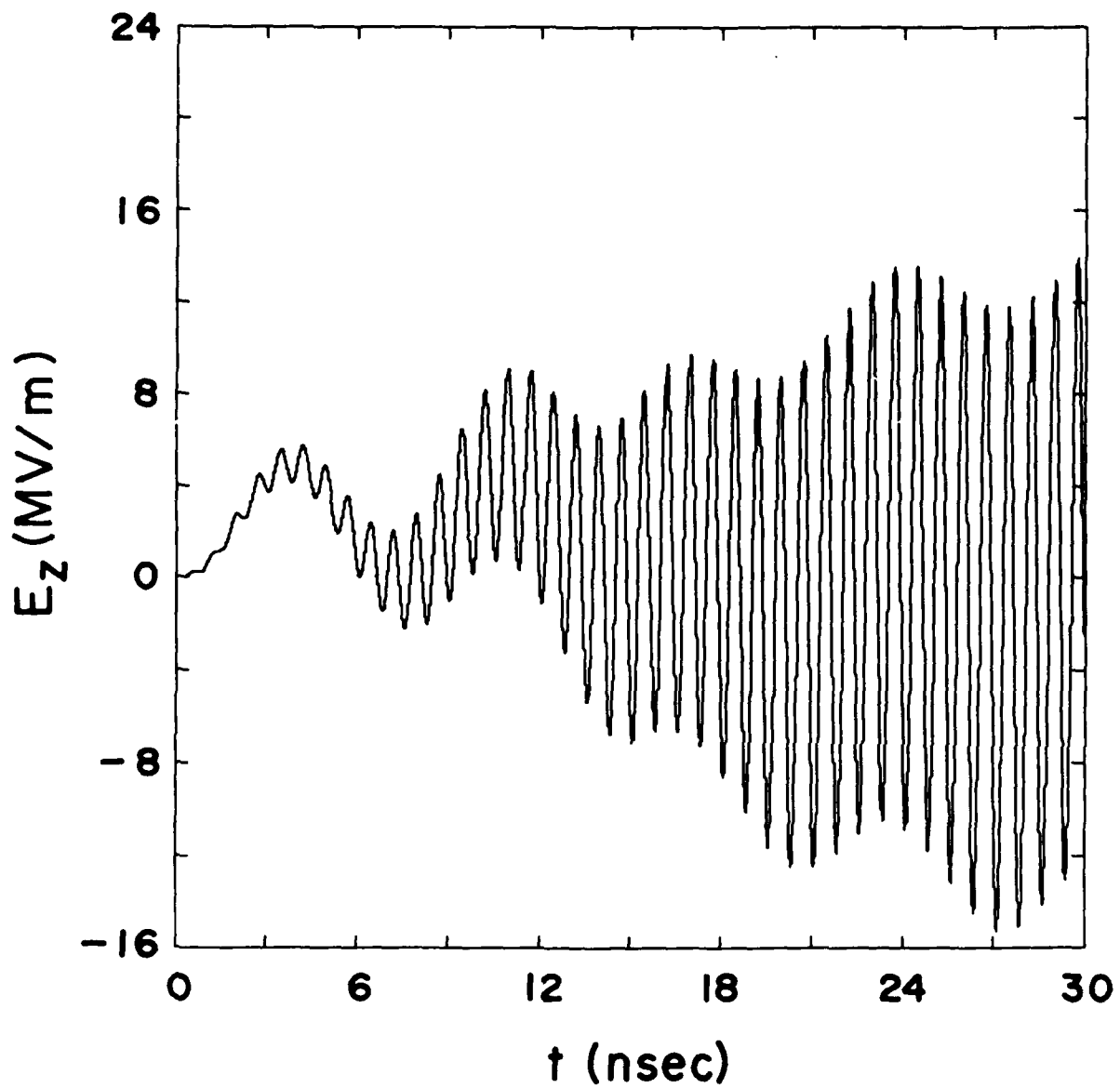


Fig. 9. E_z versus t at the gap for the $r_b = 8.0$ cm case.

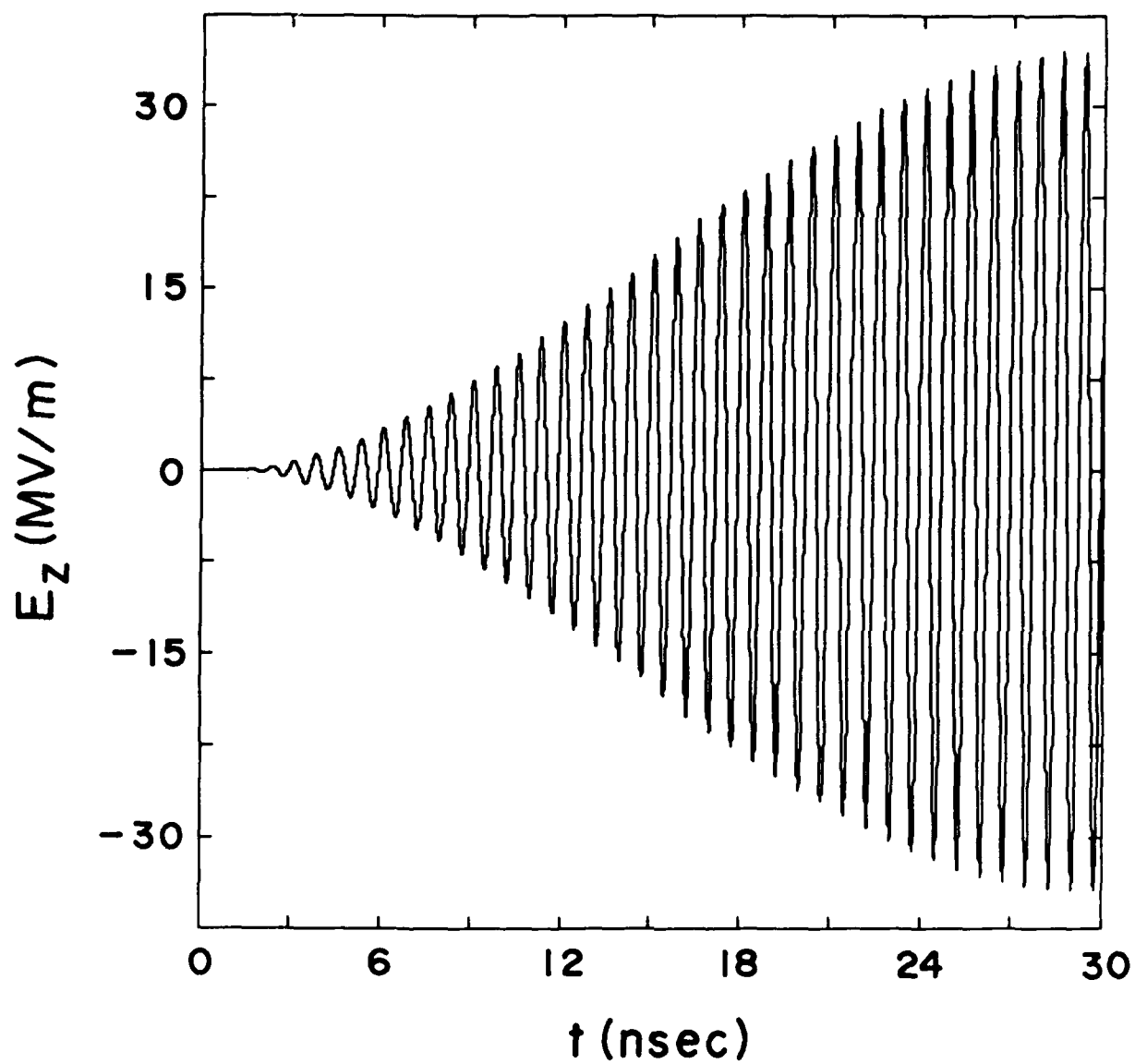


Fig. 10. E_z versus t on-axis at $z = 22.6$ cm, near the point of peak axial field.

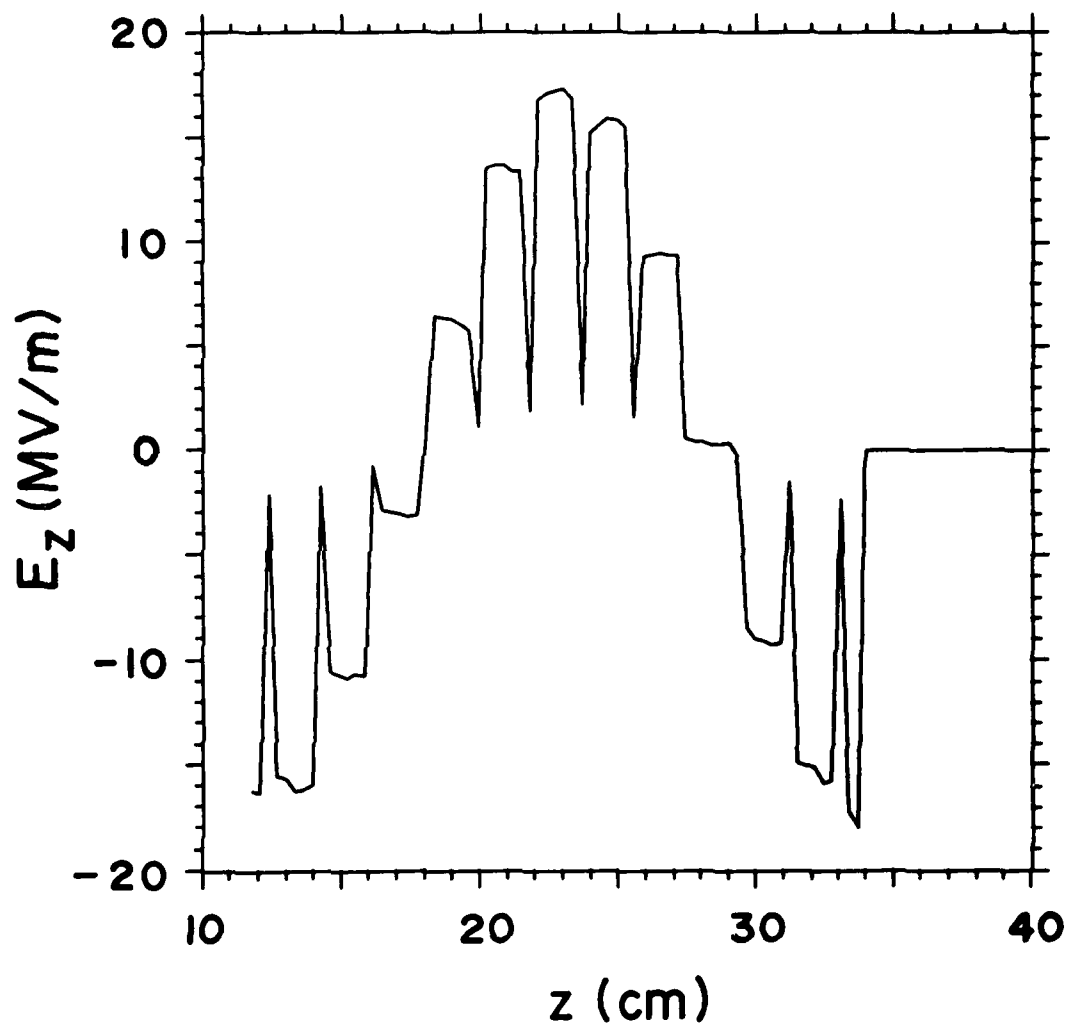


Fig. 11. E_z versus z on-axis at $t = 30.0$ ns.

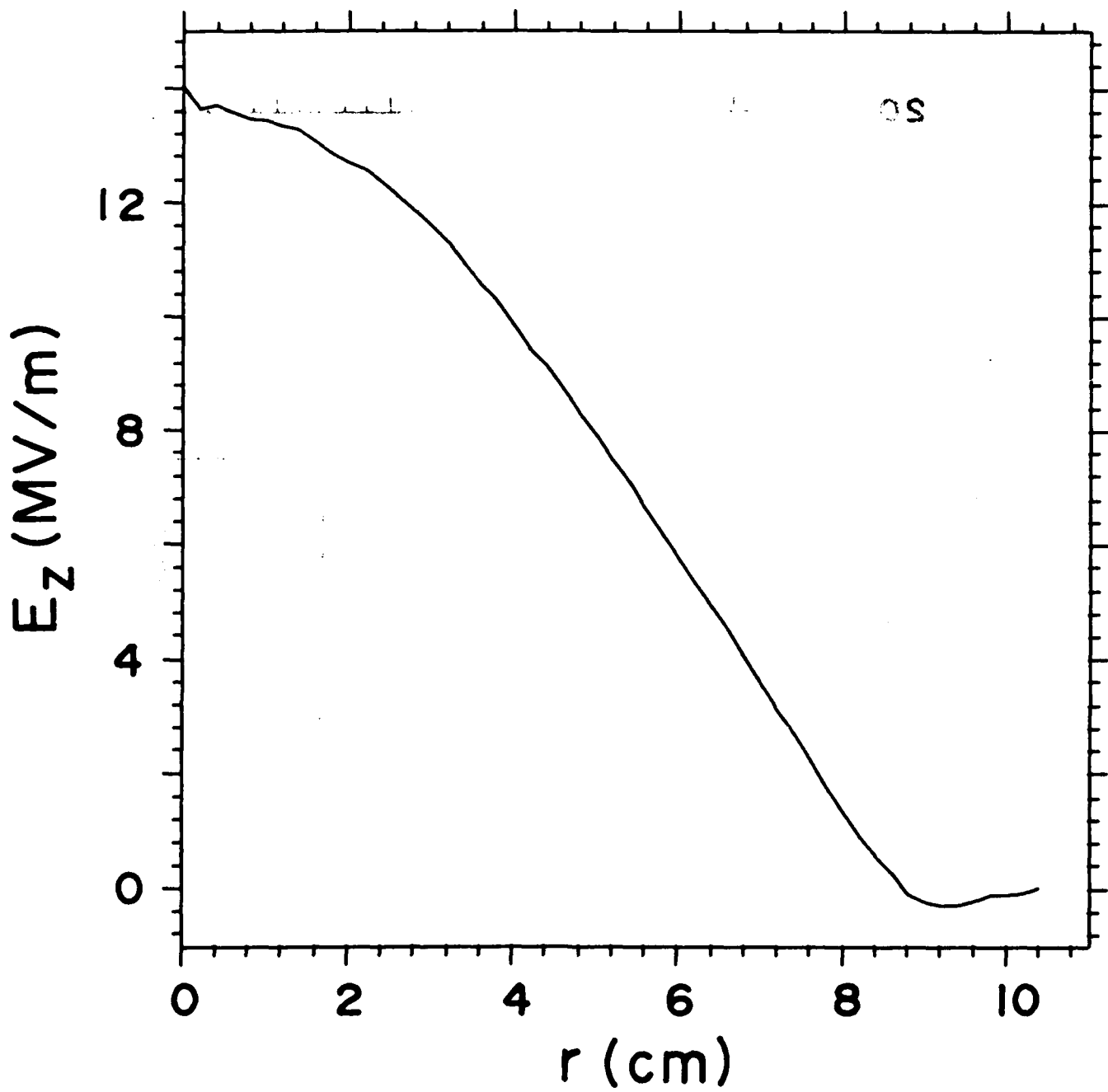


Fig. 12. E_z versus r near the point of peak axial field, $z = 20.6$ cm, at $t = 30$ ns.

DISTRIBUTION LIST

Naval Research Laboratory
4555 Overlook Avenue, S.W.
Washington, DC 20375-5000

Attn: Code 1000 - Commanding Officer, CAPT W. G. Clautice
1001 - Dr. T. Coffey
1005 - Head, Office of Management & Admin.
1220 - Mr. M. Ferguson
2000 - Director of Technical Services
2604 - NRL Historian
2628 - Documents (22 copies)
2634 - D. Wilbanks
4000 - Dr. W. R. Ellis
4600 - Dr. D. Nagel
4603 - Dr. W. W. Zachary
4700 - Dr. S. Ossakow (26 copies)
4700.1 - Dr. M. Friedman (5 copies)
4700.1 - V. Serlin
4710 - Dr. J. A. Pasour
4710 - Dr. C. A. Kapetanakis
4730 - Dr. R. Elton
4730 - Dr. B. Ripin
4740 - Dr. W. M. Manheimer
4740 - Dr. S. Gold
4790 - Dr. P. Sprangle
4790 - Dr. C. M. Tang
4790 - Dr. M. Lampe
4790 - Dr. Y. Y. Lau (40 copies)
4790 - Dr. G. Joyce
4790 - Dr. I. Haber
4790 - Dr. R. Fernsler
4790 - Dr. S. Slinker
4790 - Dr. T. Godlove
4790A- B. Pitcher
6840 - Dr. S. Y. Ahn
6840 - Dr. A. Ganguly
6840 - Dr. R. K. Parker
6843 - Dr. N. R. Vanderplaats
6875 - Dr. R. Wagner

* Every name listed on distribution gets one copy except for those where extra copies are noted.

Prof. I. Alexeff
Dept. of Electrical Engineering
University of Tennessee
Knoxville, TN 37996-2100

Dr. Bruce Anderson
Lawrence Livermore National Laboratory
L-436
P. O. Box 808
Livermore, CA 94550

Dr. T. Antonsen
University of Maryland
College Park, MD 20742

Assistant Secretary of the
Air Force (RD&L)
Room 4E856, The Pentagon
Washington, D.C. 20330

Dr. W. A. Barletta
Lawrence Livermore National Lab.
P. O. Box 808
Livermore, CA 94550

Dr. L. R. Barnett
3053 Merrill Eng. Bldg.
University of Utah
Salt Lake City UT 84112

Dr. Robert Behringer
Office of Naval Research
1030 E. Green
Pasadena, CA 91106

Dr. G. Bekefi
Mass. Institute of Tech.
Bldg. 26
Cambridge, MA 02139

Prof. Herbert Berk
Institute for Fusion Studies
University of Texas
Austin, TX 78712

Dr. T. Berlincourt
Office of Naval Research
Attn: Code 420
Arlington, VA 22217

Dr. I. B. Bernstein
Mason Laboratory
Yale University
400 Temple Street
New Haven, CT 06520

Prof. A. Bers
Dept. of Electrical Engineering
MIT
Cambridge, MA 02139

Prof. Charles K. Birdsall
Dept. of Electrical Engineering
University of California
Berkeley, CA 94720

Dr. H. Brandt
Department of the Army
Harry Diamond Laboratory
2800 Powder Mill Rd.
Adelphi, MD 20783

Dr. Charles Brau
Los Alamos National Scientific
Laboratory
P.O. Box 1663, M.S. - 817
Los Alamos, NM 87545

Dr. R. Briggs
Lawrence Livermore National Lab.
Attn: (L-71)
P.O. Box 808
Livermore, CA 94550

Prof. O. Buneman
ERL, Stanford University
Stanford, CA 94305

Dr. K. J. Button
Francis Bitter Natl. Magnet Lab.
Mass. Institute of Technology
Cambridge, MA 02139

Dr. J. A. Byers
Lawrence Livermore National Lab.
Attn: (L-630)
P. O. Box 808
Livermore, CA 94550

Prof. J. D. Callen
Nuclear Engineering Dept.
University of Wisconsin
Madison, WI 53706

Dr. Malcolm Caplan
Lawrence Livermore National Laboratory
P. O. Box 808
Livermore, CA 94550

Dr. Maria Caponi
TRW, Building R-1, Room 1184
One Space Park
Redondo Beach, CA 90278

Dr. V. S. Chan
GA Technologies
P.O. Box 85608
San Diego, CA 92138

Prof. Frank Chen
School of Eng. & Applied Sciences
Univ. of Calif. at Los Angeles
7731 K Boelter Hall
Los Angeles, CA 90024

Dr. D. P. Chernin (3 copies)
Science Applications Intl. Corp.
1720 Goodridge Drive
McLean, VA 22102

Prof. M. V. Chodorow
Ginzton Laboratory
Stanford, University
Stanford, CA 94305

Dr. William Colson
Berkeley Research Asso.
P. O. Box 241
Berkeley, CA 94701

Dr. William Condell
Office of Naval Research
Attn: Code 421
800 N. Quincy St.
Arlington, VA 22217

Dr. Richard Cooper
Los Alamos National Scientific
Laboratory
P.O. Box 1663
Los Alamos, NM 87545

Prof. B. Coppi
Dept. of Physics, 26-217
MIT
Cambridge, MA 02139

Dr. Bruce Danly
MIT
NW16-174
Cambridge, MA 02139

Dr. R. Davidson
Plasma Fusion Center
Mass. Institute of Tech.
Cambridge, MA 02139

Dr. John Dawson
Physics Department
University of California
Los Angeles, CA 90024

Dr. David A. G. Deacon
Deacon Research
Suite 203
900 Welch Road
Palo Alto, CA 94306

Deputy Under Secretary of
Defense for R&AT
Room 3E114, The Pentagon
Washington, D.C. 20301

Dr. W. W. Destler
Dept. of Electrical Engineering
University of Maryland
College Park, MD 20742

Prof. P. Diament
Dept. of Electrical Engineering
Columbia University
New York, NY 10027

Director of Research (2 copies)
U. S. Naval Academy
Annapolis, MD 21402

Dr. Gunter Dohler
Northrop Corporation
Defense Systems Division
600 Hicks Road
Rolling Meadows, IL 60008

Dr. Franklin Dolezal
Hughes Research Laboratory
3011 Malibu Canyon Rd.
Malibu, CA 90265

Dr. A. Drobot
Science Applications Intl. Corp.
1710 Goodridge Road
McLean, VA 22102

Dr. Dwight Duston
Strategic Defense Initiative Org.
OSD/SDIO/IST
Washington, DC 20301-7100

Dr. Luis R. Elias
Quantum Institute
University of California
Santa Barbara, CA 93106

Dr. W. Fawley
L-626
Lawrence Livermore National Laboratory
P. O. Box 808
Livermore, CA 94550

Dr. F. S. Felber
11011 Torrynana Road
San Diego, CA 92121

Dr. H. Fleischmann
Cornell University
Ithaca, NY 14850

Dr. Lazar Friedland
Dept. of Eng. & Appl. Science
Yale University
New Haven, CT 06520

Dr. R. Gajewski (5 copies)
Div. of Advanced Energy Projects
U. S. Dept of Energy
Washington, DC 20545

Dr. Richard L. Garwin
IBM, T. J. Watson Research Ctr.
P.O. Box 218
Yorktown Heights, NY 10598

Prof. Ward Getty
University of Michigan
Ann Arbor, MI 48109

Prof. Ronald Gilgenbach
Dept. Nucl. Engineering
University of Michigan
Ann Arbor, MI 48109

Dr. R. L. Gluckstern
Physics Department
University of Maryland
College Park, MD 20742

Dr. B. B. Godfrey
Mission Research Corporation
1720 Randolph S.E.
Albuquerque, NM 87106

Dr. V. L. Granatstein
Dept. of Electrical Engineering
University of Maryland
College Park, MD 20742

Dr. R. Harvey
Hughes Research Laboratory
3011 Malibu Canyon Road
Malibu, CA 90265

Prof. Herman A. Haus
Mass. Institute of Technology
Rm. 36-351
Cambridge, MA 02139

Dr. William Herrmannsfeldt
Stanford Linear Accelerator Center
P. O. Box 4349
Stanford, CA 94305

Dr. Fred Hopf
Optical Sciences Building, Room 602
University of Arizona
Tucson, AZ 85721

Dr. Bertram Hui
Naval Surface Warfare Center
White Oak
Silver Spring, MD 20903

Dr. Stanley Humphries, Jr.
Dept. Chemical & Nuclear Engineering
University of New Mexico
Albuquerque, NM 87131

Dr. G. L. Johnston
NW 16-232
Mass. Institute of Tech.
Cambridge, MA 02139

Dr. Howard Jory
Varian Associates, Bldg. 1
611 Hansen Way
Palo Alto, CA 94303

Prof. Terry Kammash
University of Michigan
Ann Arbor, MI 48109

Prof. Donald Kerst
3291 Chamberlin Hall
University of Wisconsin
Madison, WI 53706

Dr. K. J. Kim, MS-101
Lawrence Berkeley Lab.
Rm. 223, B-80
Berkeley, CA 94720

Dr. A. Kolb
Maxwell Laboratories, Inc.
8835 Balboa Avenue
San Diego, CA 92123

Dr. J. Krall (25 copies)
Science Applications Intl. Corp.
1710 Goodridge Drive
McLean, VA 22102

Prof. N. M. Kroll
Department of Physics
B-019, UCSD
La Jolla, CA 92093

Dr. S. P. Kuo
Polytechnic Institute of NY
Route 110
Farmingdale, NY 11735

Dr. Thomas Kwan
Los Alamos National Scientific
Laboratory, MS608
P. O. Box 1663
Los Alamos, NM 87545

Dr. Edward P. Lee
Lawrence Berkeley Laboratory
1 Cyclotron Road
Berkeley, CA 94720

Dr. Willis Lamb
Optical Sciences Center
University of Arizona
Tucson, AZ 87521

Dr. Rulon K. Linford
CTR-11, Mail Stop: 646
Los Alamos National Laboratory
P. O. Box 1663
Los Alamos, NM 87545

Dr. John Madey
S.P.R.C.
Physics Department
Stanford University
Stanford, CA 94305

Dr. J. A. Mangano
Science Research Laboratory
15 Ward Street
Sommerville, MA 02143

Dr. J. Mark
Lawrence Livermore National Lab.
Attn: L-477
P. O. Box 808
Livermore, CA 94550

Dr. W. E. Martin
L-436
Lawrence Livermore National Lab.
P. O. Box 808
Livermore, CA 94550

Dr. A. Mondelli
Science Applications Intl. Corp.
1710 Goodridge Drive
McLean, VA 22102

Prof. George Morales
Dept. of Physics
U.C.L.A.
Los Angeles, CA 90024

Dr. Philip Morton
BIN26
Stanford Linear Accelerator Center
P.O. Box 4349
Stanford, CA 94305

Dr. J. Nation
Cornell University
Ithaca, NY 14850

Dr. Kelvin Neil
Lawrence Livermore National Lab.
Code L-321, P.O. Box 808
Livermore, CA 94550

Dr. T. Orzechowski
L-436
Lawrence Livermore National Lab.
P. O. Box 808
Livermore, CA 94550

Prof. E. Ott
Department of Physics
University of Maryland
College Park, MD 20742

Dr. Robert B. Palmer
Brookhaven National Laboratories
Associated Universities, Inc.
Upton, L.I., NY 11973

Dr. W. K. H. Panofsky
Stanford Linear Accelerator Center
P. O. Box 4349
Stanford, CA 94305

Dr. Richard H. Pantell
Stanford University
Stanford, CA 94305

Dr. Dennis Papadopoulos
Astronomy Department
University of Maryland
College Park, Md. 20742

Dr. R. R. Parker
NW16-288
Plasma Fusion Center
MIT
Cambridge, MA 02139

Dr. C. K. N. Patel
Bell Laboratories
Murray Hill, NJ 07974

Dr. Richard M. Patrick
AVCO Everett Research Lab., Inc.
2385 Revere Beach Parkway
Everett, MA 02149

Dr. Claudio Pellegrini
Brookhaven National Laboratory
Associated Universities, Inc.
Upton, L.I., NY 11973

Dr. Sam Penner
National Bureau of Standards,
RADP B102
Washington, DC 20234

Dr. Hersch Pilloff
Code 1112
Office of Naval Research
Arlington, VA 22217

Dr. Donald Prosnitz
Lawrence Livermore National Lab.
Attn: L-470
P. O. Box 808
Livermore, CA 94550

Dr. M. Reiser
University of Maryland
Department of Physics
College Park, MD 20742

Dr. S. Ride
Johnson Space Center
Houston, TX 77058

Dr. C. W. Roberson (5 copies)
Code 1112
Office of Naval Research
800 N. Quincy Street
Arlington, VA 22217

Dr. Marshall N. Rosenbluth
Institute for Fusion Studies
The Univ. of Texas at Austin
Austin, TX 78712

Dr. N. Rostoker
University of California
Department of Physics
Irvine, CA 92717

Dr. J. Scharer
ECE Dept.
Univ. of Wisconsin
Madison, WI 53706

Dr. E. T. Scharlesmann
L626
Lawrence Livermore National Laboratory
P. O. Box 808
Livermore, CA 94550

Dr. Michael Schlesinger
ONR Code 1112
800 N. Quincy Street
Arlington, VA 22217-5000

Prof. S. P. Schlesinger
Dept. of Electrical Engineering
Columbia University
New York, NY 10027

Dr. Howard Schlossberg
AFOSR
Bolling AFB
Washington, D.C. 20332

Dr. George Schmidt
Stevens Institute of Technology
Physics Department
Hoboken, NJ 07030

Dr. H. Schwettmann
Phys. Dept. & High Energy
Physics Laboratory
Stanford University
Stanford, CA 94305

Dr. Marlan O. Scully
Dept. of Physics & Astronomy
Univ. of New Mexico
800 Yale Blvd. NE
Albuquerque, NM 87131

Dr. A. M. Sessler
Lawrence Berkeley Laboratory
University of California
1 Cyclotron Road
Berkeley, CA 94720

Dr. W. Sharp
L-626
Lawrence Livermore National Laboratory
P. O. Box 808
Livermore, CA 94550

Dr. R. Shefer
Science Research Laboratory
15 Ward Street
Somerville, MA 02143

Dr. Shen Shey (2 copies)
DARPA/DEO
1400 Wilson Boulevard
Arlington, VA 22209

Dr. D. J. Sigmar
Oak Ridge National Laboratory
P. O. Box Y
Oak Ridge, TN 37830

Dr. Jack Slater
Spectra Technology
2755 Northup Way
Bellevue, WA 98004

Dr. Lloyd Smith
Lawrence Berkeley Laboratory
University of California
1 Cyclotron Road
Berkeley, CA 94720

Dr. R. Sudan
Cornell University
Ithaca, NY 14850

Dr. David F. Sutter
ER 224, GTN
Department of Energy
Washington, D.C. 20545

Dr. T. Tajima
IFS
Univ. of Texas
Austin, TX 78712

Dr. R. Temkin
Mass. Institute of Technology
Plasma Fusion Center
Cambridge, MA 02139

Dr. Keith Thomassen, L-637
Lawrence Livermore National Laboratory
P. O. Box 808
Livermore, CA 94550

Dr. K. Tsang
Science Applications Intl. Corp.
1710 Goodridge Drive
McLean, VA 22102

Dr. H. S. Uhm
Naval Surface Warfare Center
White Oak Lab.
Silver Spring, MD 20903

Under Secretary of Defense (R&E)
Office of the Secretary of Defense
Room 3E1006, The Pentagon
Washington, D.C. 20301

Dr. J. Walsh
Physics Department
Dartmouth College
Hanover, NH 03755

Ms. Bettie Wilcox
Lawrence Livermore National Lab.
ATTN: Tech. Info. Dept. L-3
P.O. Box 808
Livermore, CA 94550

Dr. Perry Wilson
Stanford Linear Accelerator Center
P. O. Box 4349
Stanford, CA 94305

Dr. J. Wurtele
M.I.T.
NW 16-234
Plasma Fusion Center
Cambridge, MA 02139

Dr. A. Yariv
California Institute of Tech.
Pasadena, CA 91125

Dr. S. S. Yu
L-626
Lawrence Livermore National Laboratory
P. O. Box 808
Livermore, CA 94550